X-ray Structural and Imidazole-Binding Studies of Nickel β-Oxoporphyrins

Patricia A. Connick, Kenneth J. Haller, and Kathleen A. Macor*

Department of Chemistry and Biochemistry, University of Notre Dame, Notre Dame, Indiana 46556

Received October 1, 1992

X-ray structures for [3,3,8,8,12,13,17,18-octaethyl-3*H*,8*H*-porphine-2,7-dionato(2–)]nickel (nickel di-β-oxoporphyrin-II, NiDP-II) (**2**) and [3,3,7,8,12,12,18,18-octaethyl-3*H*,12*H*,18*H*-porphine-2,13,17-trionato(2–)]nickel (nickel tri-β-oxoporphyrin-A, NiTP-A) (**3**) are reported for the first time along with a structure of higher precision for the previously studied complex [3,3,7,8,12,13,17,18-octaethyl-3*H*-porphin-2-onato(2–)]nickel (nickel mono-β-oxoporphyrin, NiMP) (**1**) (Stolzenberg, A. M.; Glazer, P. A.; Foxman, B. M. *Inorg. Chem.* **1986**, *25*, 983–991). Average methine carbon displacements from the four-nitrogen plane increase with increasing number of β-oxo groups: <0.10 Å (NiMP, general), 0.35 Å (NiMP, special), 0.45 Å (NiDP-II), and 0.52 Å (NiTP-A). These values correlate with the decreased aromaticity and concomitant greater ring flexibility which result from the presence of one, two, or three β-oxo substituents. NiMP shows essentially no tendency to bind imidazole, whereas K_1 and K_2 values for imidazole binding are 10 ± 4 and 7 ± 2 M^{-1} for NiDP-II and 1700 ± 300 and 500 ± 150 M^{-1} for NiTP-A. The structural mechanism for the parallel increases in ring ruffling and strength of imidazole binding is the significant flexibility of the β-oxoporphyrin rings, which facilitates the core expansion and ring flattening accompanying formation of 6-coordinate high-spin Ni(II). NiTP-A exhibits a higher affinity for imidazole than positively charged porphyrins and the Ni-containing tetrahydrocorphin Factor 430. $Ni^{3+/2+}$ potentials of NiDP-II and NiTP-A are sensitive to imidazole concentration, shifting in the negative direction as imidazole is added, which indicates imidazole ligation preferentially stabilizes Ni(III). Ni^{II}TP-A is oxidized to the Ni(III) complex at 0.27 V vs SCE in the presence of imidazole, 0.36 V lower than the value for $Ni^{3+/2}$ oxidation in methylene chloride solution. This result illustrates the powerful modulation of $Ni^{3+/2+}$ potentials which can be accomplished by a biologically relevant porphyrinic ligand. Crystallographic data are as follows. NiMP: monoclinic space group $C2/c$, a = 38.549(9) Å, b = 14.744(5) Å, c = 17.329(4) Å, β = 102.47(2)°, V = 9617(8) Å^3, Z = 12, R_F = 0.079 and R_{wF} = 0.102, based on 6914 unique data points with $F_o > 3\sigma(F_o)$, T = 294 ± 1 K. NiDP-II: monoclinic space group $P2_1/c$, a = 12.370(1) Å, b = 17.199(3) Å, c = 15.172(1) Å, β = 91.09(1)°, V = 3227.4(6) Å^3, Z = 4, R_F = 0.044 and R_{wF} = 0.057, based on 6012 unique data points with $F_o > 3\sigma(F_o)$, T = 294 ± 1 K. NiTP-A: monoclinic space group $P2_1/c$, a = 11.880(1) Å, b = 23.301(3) Å, c = 12.585(1) Å, β = 106.03(2)°, V = 3348.4(9) Å^3, Z = 4, R_F = 0.088 and R_{wF} = 0.076, based on 3576 unique data points with $F_o > 3\sigma(F_o)$, T = 294 ± 1 K.

Introduction

An iron analog of the di-β-oxoporphyrin-II ring[1] (**2**, Figure 1) is found in heme-d_1 of *Pseudomonas aeruginosa* and *Paracoccus denitrificans* nitrite reductases,[2] a class of enzymes which reduces nitrite to nitric oxide.[3] Recently, a second naturally occurring di-β-oxoporphyrin was identified.[4] Tolyporphin, a derivative of di-β-oxoporphyrin-V,[1] has been isolated from *Tolypothrix nodosa*, a blue-green alga, and has been shown to have potent multidrug resistance reversibility activity.[4] It is of considerable interest to determine the β-oxoporphyrin properties which facilitate their biological roles in order to better understand the biological systems and to provide a basis for utilizing this porphyrinic class in possible electrochemical and catalytic schemes.

The pioneering work of Inhoffen and Nolte[5] and recent work from our laboratory[6] and the laboratories of Fajer,[7] Stolzenberg,[8] Loehr,[9,10] Andersson,[10] and Montforts[11] have demonstrated that the β-oxoporphyrins have unique structural,[6,11] electrochemical,[6,7b,8] electronic,[5–8] and vibrational[6,9,10] spectroscopic properties. The distinctive ring ruffling observed in the nickel di-β-oxo-[6,11] and tri-β-oxoporphyrin[6] structures distinguishes β-oxoporphyrins from porphyrins and identifies them as members of the reduced porphyrinic series, comprising chlorins, bacteriochlorins, isobacteriochlorins, corphins, pyrrocorphins, etc. This series has been intensely studied[12] in order to model F430, the nickel-containing

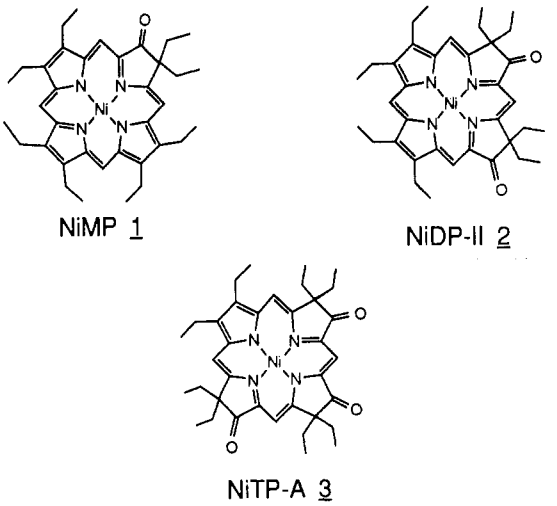

Figure 1. Structures of NiMP, NiDP-II, and NiTP-A.

* Author to whom correspondence should be addressed.

(1) Nomenclature originates from the pioneering work of Inhoffen and Nolte.[5]
(2) Chang, C. K. *J. Biol. Chem.* **1985**, *260*, 9520–9522.
(3) Kuronen, T.; Ellfolk, N. *Biochim. Biophys. Acta* **1972**, *275*, 308–318.
(4) Prinsep, M. R.; Caplan, F. R.; Moore, R. E.; Patterson, G. M.; Smith, C. D. *J. Am. Chem. Soc.* **1992**, *114*, 385–387.
(5) Inhoffen, H.; Nolte, W. *Justus Liebigs Ann. Chem.* **1969**, *725*, 167–176.
(6) Connick, P. A.; Macor, K. A. *Inorg. Chem.* **1991**, *30*, 4654–4663.
(7) (a) Barkigia, K. M.; Chang, C. K.; Fajer, J.; Renner, M. W. *J. Am. Chem. Soc.* **1992**, *114*, 1701–1701. (b) Chang, C. K.; Barkigia, K. M.; Hanson, L. K.; Fajer, J. *J. Am. Chem. Soc.* **1986**, *108*, 1352–1354.
(8) Stolzenberg, A. M.; Glazer, P. A.; Foxman, B. M. *Inorg. Chem.* **1986**, *25*, 983–991.
(9) Andersson, L. A.; Loehr, T. M.; Wu, W.; Chang, C. K.; Timkovich, R. *FEBS Lett.* **1990**, *267*, 285–288.
(10) Mylrajan, M.; Andersson, L.A.; Loehr, T. M.; Wu, W.; Chang, C. K. *J. Am. Chem. Soc.* **1991**, *113*, 5000–5005.
(11) Montforts, F. P.; Romanowski, F.; Bats, J. W. *Angew. Chem., Int. Ed. Engl.* **1989**, *28*, 480–483.

0020-1669/93/1332-3256$04.00/0

Table I. Crystal Data and Intensity Data Collection Parameters[a]

	NiMP	NiDP-II	NiTP-A
empirical formula	$C_{36}H_{44}NiN_4O$	$C_{36}H_{44}NiN_4O_2$	$C_{36}H_{44}NiN_4O_3$
fw	607.49	623.49	639.49
crystal dimens, mm	0.45 × 0.50 × 0.56	0.17 × 0.20 × 0.46	0.05 × 0.17 × 0.19
crystal color/shape	green irregular chunk	green rod-shaped needle	green irregular plate
crystal system	monoclinic	monoclinic	monoclinic
space group	$C2/c$ (No. 15)	$P2_1/c$ (No. 14)	$P2_1/c$ (No. 14)
a, Å	38.549(9)	12.370(1)	11.880(1)
b, Å	14.744(5)	17.199(3)	23.301(3)
c, Å	17.329(4)	15.172(1)	12.585(1)
β, °	102.47(2)	91.09(1)	106.03(1)
V, Å^3	9617(8)	3227.4(6)	3348.4(9)
lattice parameter refinement	25 reflns; 30.8° < 2θ < 63.0°	25 reflns; 7.6° < 2θ < 34.4°	25 reflns; 16.8° < 2θ < 63.4°
Z	12	4	4
calcd density, g/cm^3	1.26	1.28	1.27
μ(Cu Kα), cm^{-1}	10.95	11.24	11.18
ω width at half-height, deg	0.32	0.20	0.36
scan rate, deg/min in ω	4.12	2.06–4.12	3.30
scan width, deg	1.10 + 0.142 tan θ	0.50 + 0.142 tan θ	0.90 + 0.142 tan θ
2θ range, deg	3.0–156.0	3.0–156.0	3.0–136.3
(sin θ)/λ max	0.632	0.626	0.601
no. of total reflns measd	20 241	10 022	7608
no. of unique reflns measd	10 127	6741	6963
no. of unique reflns, $F_o > 3\sigma(F_o)$	6914	6012	3576
linear decay cor on I	none	1.000–1.012	1.000–1.020
reflns averaging: $R_{merge}(I)$, multiply measd data	0.065, 9262	0.032, 3049	0.035, 331
p, weight = $[\sigma^2(F)^2 + p^2F^2]^{-1/2}$	0.04	0.02	0.03
data:variable ratio	11.8	15.5	8.6
$R_1 = \sum\|F_o - F_c\|/\sum\|F_o\|$	0.079	0.044	0.088
$R_2 = [\sum w(F_o - F_c)^2/\sum wF_o^2]^{1/2}$	0.102	0.057	0.076
gof = $[\sum w(\|F_o\| - \|F_c\|)^2/(m-n)]^{1/2}$	1.77	2.92	1.64
highest peak in final diff map	0.52(7)	0.36(5)	0.44(10)

[a] T = 294 ± 1 K; Enraf-Nonius CAD4 diffractometer; graphite crystal incident beam monochromated Cu Kα X-ray source, $\bar{\lambda}$ = 1.541 84 Å; takeoff angle 2.8°; vertical aperture 4.0 mm, horizontal aperture 2.5 + 0.5 tan θ; crystal to source distance 210 mm; moving crystal—moving counter background counts at each end of the scan, scan:background 2:1; Ni foil attenuator, factor 17.956; hydrogens included as idealized fixed contributors, d(CH) = 0.95 Å, B(H) = 1.2B($C_{attached}$); full-matrix least-squares refinement based on the unique data with $F_o > 3\sigma(F_o)$, minimization function $\sum w(|F_o| - |F_c|)^2$; calculations carried out on a VAXstation 3200 using the SDP/VAX computer software system.

tetrahydrocorphin isolated from *Methanobacterium thermoautotrophicum*.[13]

Most of the research on the reduced porphyrin series has focused on axial ligand binding and $Ni^{2+/1+}$ reduction, since these appear to be key properties in the chemistry of F430. It has been aptly demonstrated that flexibility of a nickel porphyrinic ring, as measured by distortions from planarity, enhances axial ligand binding[12a,e-g,14] and is required for reduction of the Ni(II) center.[12a-c,15] Both processes require an expansion of the porphyrinic core to accept larger ions, either high-spin axially ligated Ni(II) or Ni(I).

In addition to Ni(I), Ni(III) has also been suggested as an intermediate in the F430 catalytic cycle.[16] Similar ring flexibility arguments should hold for $Ni^{3+/2+}$ oxidation, since the porphyrinic core size is altered by (i) loss of an electron from the Ni center and (ii) electron rearrangement resulting from any axial ligation change. We recently reported studies of Ni(II) β-oxooctaethylporphyrins,[6] which demonstrated that within the mono-, di-, and tri-β-oxooctaethylporphyrin series only the last is oxidized to the Ni(III) state in methylene chloride solution.

In the present paper we report the X-ray structural data for nickel di-β-oxoporphyrin-II (NiDP-II) (**2**) and nickel tri-β-oxoporphyrin-A (NiTP-A) (**3**). X-ray structural data for nickel mono-β-oxoporphyrin (NiMP) (**1**) of higher precision than previously reported[8] are also presented. Methine carbon deviations from the nitrogen plane are 0.45 and 0.52 Å in NiDP-II and NiTP-A, respectively, compared to 0.58 and approximately 0.66 Å in nickel tetramethylchlorin (NiTMC)[17] and nickel tetramethylisobacteriochlorin (NiTMiBC),[18] respectively.

In this paper we demonstrate that imidazole does not bind to NiMP but does so with increasing strength to NiDP-II and NiTP-A. K_1 equals 1700 ± 300 M^{-1} for imidazole ligation in NiTP-A, which is approximately 3 times as large as K_1 for native F430M.[19,20] Imidazole ligation is unusual in Ni porphyrins and, in fact, only occurs in the presence of positively charged porphyrins[21] or reduced porphyrinic compounds, which exhibit extensive ring ruffling, such as the tetrahydrocorphin, F430.[19] The strength of axial ligand binding in F430 has been explained by the very large flexibility of the tetrahydrocorphin ring.[14] (A value of 0.78 Å has recently been reported for the average displacement of the methine carbons from the nitrogen plane in the F430M 12, 13-diepimer.[22]) This flexibility facilitates the

(12) (a) Renner, M. W.; Furenlid, L. R.; Barkigia, K. M.; Forman, A.; Shim, H. K.; Simpson, D. J.; Smith, K. M.; Fajer, J. *J. Am. Chem. Soc.* **1991**, *113*, 6891–6898. (b) Furenlid, L. R.; Renner, M. W.; Smith, K. M.; Fajer, J. *J. Am. Chem. Soc.* **1990**, *112*, 1634–1635. (c) Stolzenberg, A. M.; Stershic, M. T. *J. Am. Chem. Soc.* **1988**, *110*, 6391–6402. (d) Shelnutt, J. A. *J. Am. Chem. Soc.* **1987**, *109*, 4169–4173. (e) Eschenmoser, A. *Ann. N.Y. Acad. Sci.* **1986**, *471*, 108–129. (f) Pfaltz, A.; Livingston, D. A.; Jaun, B.; Dickert, G.; Thauer, R. K.; Eschenmoser, A. *Helv. Chim. Acta* **1985**, *68*, 1338–1358. (g) Kratky, C.; Fassler, A.; Pfaltz, A.; Krautler, B.; Jaun, B.; Eschenmoser, A. *J. Chem. Soc., Chem. Commun.* **1984**, 1368–1371.
(13) Pfaltz, A. In *The Bioinorganic Chemistry of Nickel*; Lancaster, J. R., Ed.; VCH Publishers: New York, 1988; Chapter 12.
(14) Kratky, C.; Waditschatka, R.; Angst, C.; Johansen, J. E.; Plaquevent, J. C.; Schreiber, J.; Eschenmoser, A. *Helv. Chim. Acta* **1985**, *68*, 1312–1337.
(15) Jaun, B.; Pfaltz, A. *J. Chem. Soc., Chem. Commun.* **1986**, 1327–1329.
(16) Jaun, B. *Helv. Chim. Acta* **1990**, *73*, 2209–2217.
(17) Gallucci, J. C.; Swepston, P. N.; Ibers, J. A. *Acta Crystallogr.* **1982**, *B38*, 2134–2139.
(18) Suh, M. P.; Swepston, P. N.; Ibers, J. A. *J. Am. Chem. Soc.* **1984**, *106*, 5164–5171.
(19) Fassler, A. Diss. ETH Nr. 7799,1985.
(20) According to ref 15, F430M, the pentamethyl ester derivative, has been more extensively studied than F430, the pentacarboxylic acid, because the former is more stable, is easier to purify, and can be studied under aprotic conditions.
(21) Pasternack, R. F.; Spiro, E. G.; Teach, M. *J. Inorg. Nucl. Chem.* **1974**, *36*, 599–606.

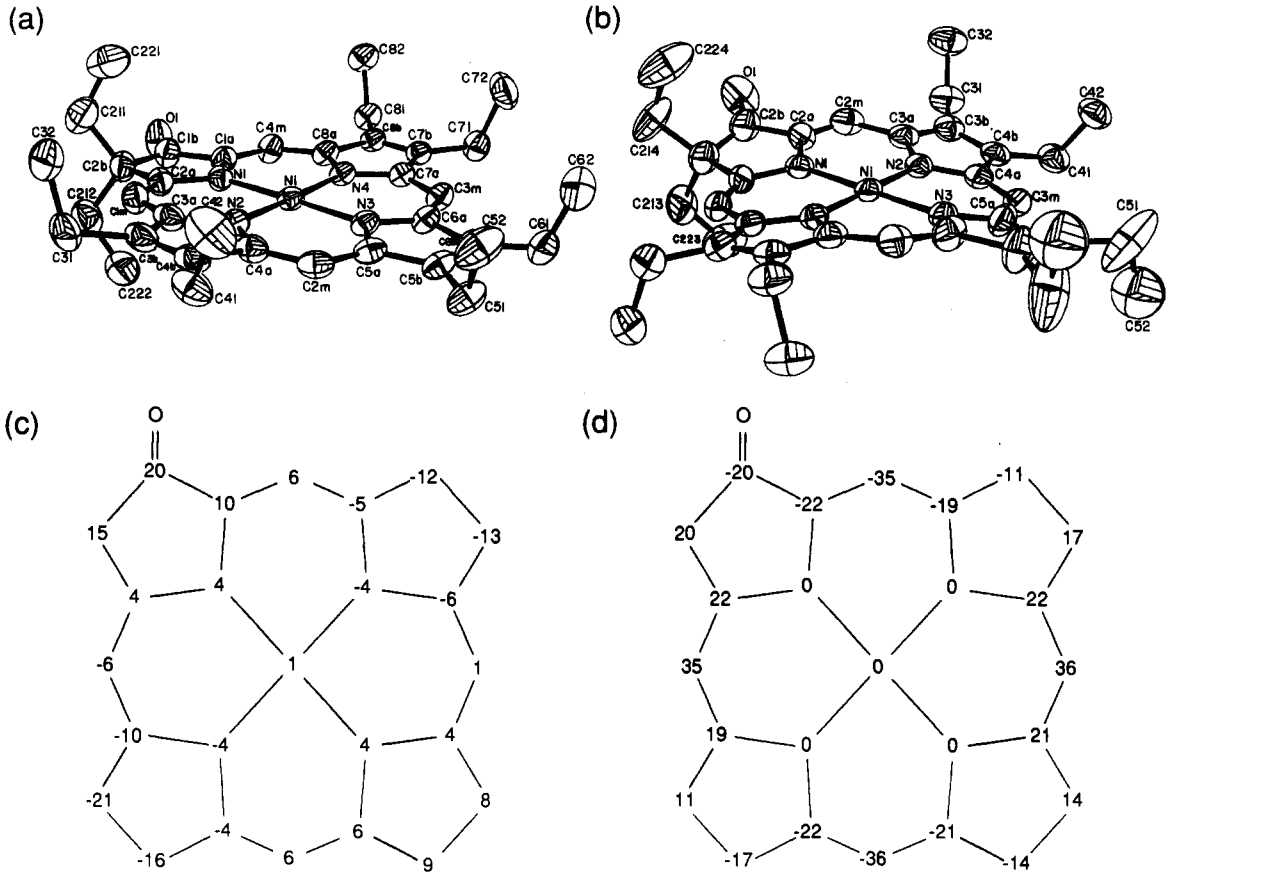

Figure 2. ORTEP drawings for (a) the general-position and (b) the special-position molecules of NiMP showing the atom-numbering scheme. Thermal ellipsoids are drawn to illustrate 30% probability surfaces. Hydrogen atoms are omitted for clarity. Deviations (Å × 10^2) from the least-squares plane of the four nitrogen atoms for (c) the general-position and (d) the special-position molecules of NiMP. Because the special-position molecule contains an axis of symmetry which passes through the nickel atom and bisects the C_β–C_β bond of the pyrrolinone ring, only half of the atoms in the crystal have independent coordinates.

expansion of the tetrahydrocorphin ring required to bind the larger high-spin Ni(II) ion by releasing the considerable conformational strain energy which exists due to ruffling. The fact that NiTP-A exhibits stronger imidazole binding, albeit less nonplanarity, than F430M suggests that NiTP-A has a greater confomational strain energy.

We also report results of electrochemical studies which show that strong imidazole binding to Ni^{III}DP-II and Ni^{III}TP-A shifts $Ni^{3+/2+}$ potentials in the negative direction. Our results show that Ni^{II}TP-A is oxidized to the Ni(III) state at 0.27 V vs SCE in the presence of imidazole, 0.36 V lower than the value for $Ni^{3+/2+}$ oxidation in methylene chloride solution.[6] This result illustrates the powerful modulation of $Ni^{3+/2+}$ potentials which can be accomplished by a biologically relevant porphyrinic ligand.

Experimental Section

Chemicals. The nickel β-oxoporphyrins used in this study were synthesized as previously described.[6] Nickel octaethylporphyrin (NiOEP) (Mid-Century Chemicals, Posen, IL) was used as received. CH_2Cl_2 (Fisher, Pittsburgh, PA) was dried over CaH_2 and distilled prior to use or was ordered as anhydrous (Aldrich, Milwaukee, WI) and used as received. Tetrabutylammonium perchlorate (TBAP) (GFS Chemicals, Columbus, OH) was recrystallized from ethyl acetate and dried *in vacuo*. Imidazole (Im) (99%, Aldrich) was used as received.

X-ray Structural Analysis. Crystals of NiMP and NiDP-II were grown at room temperature by vapor diffusion of pentane (NiMP) or hexane (NiDP-II) into a CH_2Cl_2 solution of the Ni β-oxoporphyrin. NiTP-A crystals were grown at 5 °C by vapor diffusion of pentane into a NiTP-A/CH_2Cl_2 solution.

Crystallographic data were collected using Cu Kα radiation ($\bar{\lambda}$ = 1.541 84 Å) on an Enraf-Nonius diffractometer equipped with a graphite crystal incident beam monochromator operating at 294 ± 1 K. Parameters are summarized in Table I. Empirical absorption corrections based on ψ scans were applied to the data. Scattering factors were taken from Cromer and Waber.[23] All calculations were performed using the SDP/VAX program system.[24] Positions for most of the hydrogen atoms could be found in electron density difference Fourier maps calculated after preliminary refinement of the non-hydrogen atoms. These were subsequently idealized. All structures were refined by full-matrix least-squares procedures.

Spectrophotometric Titrations. Electronic absorption spectra (350–850 nm) were recorded on a Bausch and Lomb Spectronic 1001 spectrophotometer supplied with an RS-232 interface to an IBM PC XT computer. Spectra were plotted using Galactic Industries Lab Calc software and a Hewlett-Packard Color Pro plotter.

Equilibrium constants for imidazole axial ligation were determined by the method of Rose and Drago[25] in imidazole concentration ranges where only one equilibrium was present, as indicated by isosbestic points. K_1 and K_2 describe the equilibria between the 4- and 5-coordinate species and between the 5- and 6-coordinate complexes, respectively.

K_1 was calculated from eq 1, where L_0 is the initial concentration of imidazole, C_0 is the initial β-oxoporphyrin concentration, A_0 is the

$$1/K_1 = L_0(C_0\Delta\epsilon_1/(A - A_0) - 1) \qquad (1)$$

absorbance of 4-coordinate β-oxoporphyrin solution, A is the absorbance

(22) Farber, G.; Keller, W.; Kratky, C.; Jaun, B.; Pfaltz, A.; Spinner, C.; Kobelt, A.; Eschenmoser, A. *Helv. Chim. Acta* **1991**, *74*, 697–716.

(23) Cromer, D.T.; Waber, J. T. *International Tables for X-Ray Crystallography*; Kynoch Press: Birmingham, England, 1974; Vol. IV, Table 2.2B.

(24) Frenz, B. A. In *Computing in Crystallography*; Schenk, H., Olthof-Hazelkamp, R., van Konigsveld, H., Bassi, G. C., Eds.; Delft University Press: Delft, Holland, 1978; pp 64–71.

(25) Rose, N. J.; Drago, R. S. *J. Am. Chem. Soc.* **1959**, *81*, 6138–6145.

Table II. NiMP Fractional Monoclinic Coordinates and Isotropic Atomic Displacement Parameters (Å²)[a,b]

General-Position Molecule

atom	x	y	z	B_{iso}	atom	x	y	z	B_{iso}
Ni	0.24150(2)	0.06222(4)	0.09103(4)	4.22(1)	C1m	0.1839(1)	−0.1131(3)	0.0700(3)	5.8(1)
N1	0.18931(8)	0.0498(2)	0.0687(2)	4.64(7)	C2m	0.3099(1)	−0.0844(3)	0.1131(3)	5.36(9)
N2	0.24638(8)	−0.0692(2)	0.0939(2)	4.68(7)	C3m	0.2984(1)	0.2390(3)	0.1149(3)	5.08(9)
N3	0.29278(8)	0.0750(2)	0.1093(2)	4.47(7)	C4m	0.1726(1)	0.2102(3)	0.0624(3)	5.5(1)
N4	0.23701(7)	0.1948(2)	0.0932(2)	4.33(6)	O1	0.10178(9)	0.1352(2)	0.0212(3)	8.3(1)
C1a	0.1652(1)	0.1214(3)	0.0566(3)	5.3(1)	C211	0.1102(2)	−0.0517(4)	0.0979(4)	9.5(2)
C2a	0.1702(1)	−0.0289(3)	0.0602(3)	5.4(1)	C221	0.1208(2)	−0.0190(6)	0.1768(5)	13.1(3)
C3a	0.2196(1)	−0.1327(2)	0.0865(3)	5.3(1)	C212	0.1131(2)	−0.0521(4)	−0.0448(4)	8.6(2)
C4a	0.2774(1)	−0.1200(2)	0.1057(2)	4.96(9)	C222	0.1300(2)	−0.0166(5)	−0.1104(4)	10.6(2)
C5a	0.3183(1)	0.0061(3)	0.1172(3)	4.94(8)	C31	0.2123(2)	−0.3082(3)	0.1004(3)	7.2(1)
C6a	0.3128(1)	0.1538(3)	0.1179(2)	4.93(8)	C32	0.2052(2)	−0.3224(4)	0.1836(4)	9.6(2)
C7a	0.2636(1)	0.2579(2)	0.1058(2)	4.46(8)	C41	0.2982(2)	−0.2873(3)	0.1239(3)	6.8(1)
C8a	0.2065(1)	0.2451(2)	0.0827(2)	4.79(8)	C42	0.3147(2)	−0.2979(4)	0.2079(4)	9.9(2)
C1b	0.1284(1)	0.0896(3)	0.0357(3)	6.0(1)	C51	0.3874(1)	−0.0113(3)	0.1413(3)	6.5(1)
C2b	0.1304(1)	−0.0133(3)	0.0383(3)	6.6(1)	C52	0.4006(1)	−0.0416(4)	0.2229(4)	9.2(2)
C3b	0.2346(1)	−0.2217(3)	0.0977(3)	6.1(1)	C61	0.3793(1)	0.2035(3)	0.1411(3)	6.7(1)
C4b	0.2703(1)	−0.2157(3)	0.1089(3)	5.6(1)	C62	0.3904(2)	0.2333(5)	0.2223(4)	11.6(2)
C5b	0.3538(1)	0.0437(3)	0.1295(3)	5.31(9)	C71	0.2711(1)	0.4322(3)	0.1207(3)	6.0(1)
C6b	0.3503(1)	0.1346(3)	0.1300(3)	5.40(9)	C72	0.2834(2)	0.4513(4)	0.2095(4)	9.5(2)
C7b	0.2496(1)	0.3496(2)	0.1050(2)	4.77(9)	C81	0.1871(1)	0.4153(3)	0.0868(3)	5.5(1)
C8b	0.2144(1)	0.3419(2)	0.0908(2)	4.65(8)	C82	0.1768(1)	0.4296(3)	0.1654(3)	7.0(1)

Special-Position Molecule

atom	x	y	z	B_{iso}	atom	x	y	z	B_{iso}
Ni*	1/2	−0.02611(6)	1/4	5.02(2)	C3m*	0.5185(1)	0.1342(3)	0.3915(3)	6.4(1)
N1*	1/2	−0.1587(3)	1/4	5.7(1)	O1*	0.5297(3)	−0.3721(4)	0.3338(7)	12.7(3)
N2*	0.52205(8)	−0.0262(2)	0.3615(2)	5.02(7)	C213*	0.5474(4)	−0.3570(6)	0.2728(9)	9.8(4)
N3*	1/2	0.1059(3)	1/4	5.5(1)	C214*	0.4999(4)	−0.3734(6)	0.3455(8)	11.5(4)
C2a*	0.5175(1)	−0.2134(3)	0.3093(3)	6.0(1)	C223*	0.5630(3)	−0.3115(9)	0.2134(8)	12.2(4)
C3a*	0.5364(1)	−0.0966(3)	0.4080(3)	6.0(1)	C224*	0.4654(5)	−0.3414(9)	0.367(1)	15.4(5)
C4a*	0.5265(1)	0.0472(3)	0.4135(3)	5.6(1)	C31*	0.5688(2)	−0.1302(4)	0.5531(4)	8.2(2)
C5a*	0.5070(1)	0.1624(3)	0.3136(3)	7.0(1)	C32*	0.6065(2)	−0.1496(4)	0.5509(4)	9.6(2)
C2b*	0.5132(2)	−0.3120(3)	0.2893(3)	7.9(2)	C41*	0.5518(1)	0.0830(4)	0.5617(3)	7.6(1)
C3b*	0.5501(1)	−0.0718(3)	0.4878(3)	6.3(1)	C42*	0.5861(2)	0.1357(4)	0.5643(4)	8.6(2)
C4b*	0.5432(1)	0.0195(3)	0.4917(3)	6.0(1)	C51*	0.5178(3)	0.3449(5)	0.3472(5)	17.4(3)
C5b*	0.5040(2)	0.2564(3)	0.2887(3)	8.7(2)	C52*	0.4908(4)	0.3594(9)	0.3791(8)	16.8(5)[c]
C2m*	0.5348(1)	−0.1860(3)	0.3791(3)	7.0(1)					

[a] Estimated standard deviations in the least significant digits are given in parentheses. Thermal parameters for the anisotropically refined atoms are given in the form of the isotropic equivalent displacement parameter defined as $(4/3)[a^2B_{11} + b^2B_{22} + c^2B_{33} + ab(\cos\gamma)B_{12} + ac(\cos\beta)B_{13} + bc(\cos\alpha)B_{23}]$. [b] Because the special-position molecule of NiMP (a disordered structure) contains an axis of symmetry which passes through the nickel atom and bisects the C_β–C_β bond of the pyrrolinone ring, only half the atoms in the crystal have independent coordinates. These are listed under the heading of the special-position molecule with an asterisk. The others may be generated by rotating the molecule around the axis of symmetry in the structure. [c] Atom refined with isotropic atomic displacement parameter.

of the β-oxoporphyrin solution at a particular imidazole concentration (within the 4- and 5-coordinate equilibrium), and $\Delta\epsilon_1$ is the difference in extinction coefficients between the 4- and 5-coordinate species. Values for $\Delta\epsilon_1$ and K_1 were obtained by solving eq 1 with data from pairs of absorbance curves within the first isosbestic point region of imidazole concentrations, at a particular wavelength. The $\Delta\epsilon_1$ and K_1 values obtained in this way were then averaged. Lines used in the calculation had slope differences greater than 5%. The process was repeated for several wavelengths, and final average $\Delta\epsilon_1$ and K_1 values were calculated.

K_2 was calculated from eq 2, where L_0 is the initial concentration of imidazole, C_0 is the initial β-oxoporphyrin concentration, A_1 is the

$$1/K_2 = L_0(C_0\Delta\epsilon_2/(A - A_1) - 1) \qquad (2)$$

absorbance of 5-coordinate β-oxoporphyrin solution, A is the absorbance of the β-oxoporphyrin solution at a particular imidazole concentration (within the 5- and 6-coordinate equilibrium), and $\Delta\epsilon_2$ is the difference in extinction coefficients between the 5- and 6-coordinate species. Since A_1 could not be measured directly, because a spectrum of pure 5-coordinate species was not obtainable, A_1 was calculated by adding $(\Delta\epsilon_1)C_0$ to A_0. Values for $\Delta\epsilon_2$ and K_2 were obtained by solving eq 2 with data from pairs of absorbance curves within the second isosbestic point region of imidazole concentrations, at a particular wavelength. The $\Delta\epsilon_2$ and K_2 values obtained in this way were then averaged. Lines used in the calculation had slope differences greater than 5%. The process was repeated for several wavelengths, and final average $\Delta\epsilon_2$ and K_2 values were calculated.

Error values for K_1 and K_2 were calculated by determining the standard deviations of the average values from the different wavelengths.

UV–vis data for NiDP-II [λ_{max}, nm (ϵ_λ)]: 387 (33 000), 437 (33 000), 577 s (10 000), 620 (32 000). UV–vis data for NiTP-A [λ_{max}, nm (ϵ_λ)]: 356 (15 000), 430 (23 000), 471 s (9300), 624 s (5500), 645 s (7800), 662 s (9900), 680 (12 000), 695 s (10 000), 731 (37 000).

Cyclic Voltammetry. Cyclic voltammograms (CV's) were obtained with a Princeton Applied Research Model 173 potentiostat, Model 179 coulometer, and Model 175 universal programmer and a Yokagawa 3025 A4 X-Y recorder. The cyclic voltammetry cell contained a Pt foil working electrode, a platinum wire counter electrode, and an aqueous (saturated KCl) calomel reference electrode positioned in a Luggin capillary. The supporting electrolyte was 0.1 M TBAP. The scan rate was 50 mV/s.

Results

X-ray Structures of NiMP, NiDP-II, and NiTP-A. Molecular structures and deviations from the plane defined by the four nitrogens are presented in Figures 2–4 for NiMP (**1**), NiDP-II (**2**), and NiTP-A (**3**), respectively. Fractional coordinates are found in Table II for NiMP, Table III for NiDP-II, and Table IV for NiTP-A. Table V contains selected bond distances and bond angles for the three compounds.

In NiMP eight molecules occupy a general position and four molecules are disordered, lying in a special position with a 2-fold axis that bisects the saturated C_β–C_β bond. Bond distance errors in the present NiMP structure have been reduced by a factor of 6 compared to those of the previously reported structure,[8] which

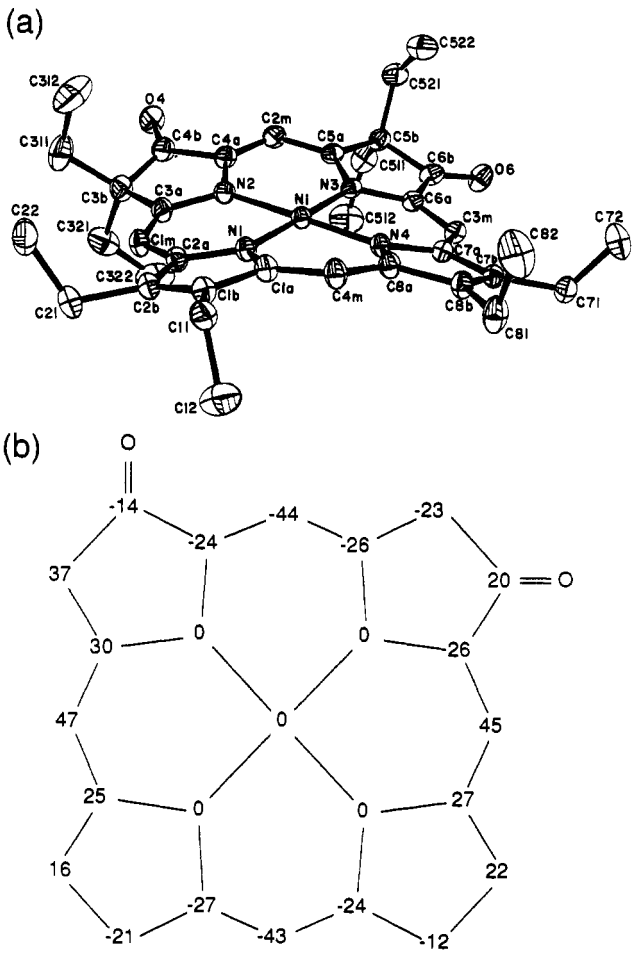

Figure 3. (a) ORTEP drawing of NiDP-II showing the atom-numbering scheme. Thermal ellipsoids are drawn to illustrate 30% probability surfaces. Hydrogen atoms are omitted for clarity. (b) Deviations (Å × 10^2) from the least-squares plane of the four nitrogen atoms for NiDP-II.

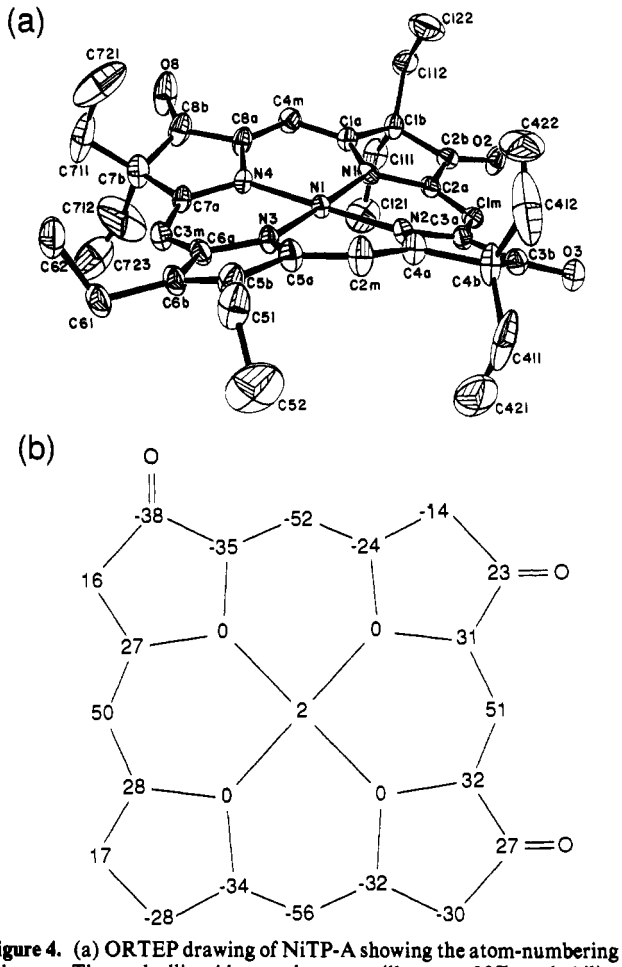

Figure 4. (a) ORTEP drawing of NiTP-A showing the atom-numbering scheme. Thermal ellipsoids are drawn to illustrate 30% probability surfaces. Hydrogen atoms are omitted for clarity. (b) Deviations (Å × 10^2) from least-squares plane of the four nitrogen atoms for NiTP-A.

has allowed us to identify trends in methine carbon deviations from planarity within the Ni β-oxooctaethylporphyrin series.

Figure 2 shows that in the NiMP general-position molecule the pyrrole/pyrrolinone rings are displaced alternately above and below the nitrogen plane. In contrast, Figures 2–4 show that the NiMP special-position molecule, NiDP-II, and NiTP-A have structures with C_β–C_α–C_m–C_α–C_β regions displaced alternately above and below the nitrogen plane in an S_4 saddle-shaped pattern. The methine carbon displacements are large in the latter three structures, 0.354(5) Å (NiMP special), 0.449(8) Å (NiDP-II), and 0.519(4) Å (NiTP-A), and increase with increasing number of β-oxo groups.

In addition to ruffling, other characteristics common to reduced porphyrinic rings[12a,14,17,18,26] are also seen in the molecular structures of **1–3**. Longer C_β–C_β bond lengths are observed in pyrrolinone versus pyrrole rings: 1.520(5) Å vs 1.343(5) Å in NiMP (general), 1.51(1) Å vs 1.355(22) Å in NiMP (special), 1.504(8) Å vs 1.358(5) Å in NiDP-II, and 1.504(6) Å vs 1.371(8) Å in NiTP-A. Longer Ni–N bonds to pyrrolinone rings versus pyrrole rings are also seen, because of wider C_α–N–C_α angles which result from the longer C_β–C_β bonds. Ni–N bond lengths to pyrrolinone versus pyrrole rings are as follows: NiMP (general), 1.973(3) Å vs 1.951(6) Å; NiMP (special), 1.955(4) Å vs 1.939(3) Å; NiDP-II, 1.957(9) Å vs 1.937(5) Å; NiTP-A, 1.961(9) Å vs 1.919(4) Å.

Conjugation of C=O groups with the porphyrinic ring is indicated by shorter pyrrolinone C_α–C_β bonds bearing the C=O group compared to C_α–C_β bonds bearing ethyl substituents. Pyrrolinone C_α–C_β (C=O) versus C_α–C_β (ethyl) bond lengths are as follows: NiMP (general):[27] 1.466(5) Å vs 1.516(5) Å; NiDP-II, 1.470(6) Å vs 1.511(2) Å; NiTP-A, 1.457(7) vs 1.509(7) Å.

Imidazole Binding to Ni β-Oxoporphyrins. Imidazole binding to Ni(II) β-oxoporphyrins was evaluated by the spectrophotometric titration method utilizing the approach of Rose and Drago.[25] The electronic absorption spectrum of NiMP showed essentially no change upon addition of large amounts of imidazole, indicating that significant imidazole binding does not occur.

Figure 5 shows that the electronic absorption spectrum of NiDP-II undergoes substantial changes when imidazole is added. NiDP-II in CH_2Cl_2 (solid line) exhibits two strong bands in the Soret region at 387 and 437 nm which shift to the red by 14 and 22 nm, respectively, in the presence of imidazole (dotted line). The two bands in the "Q band" region at 577 and 620 nm show similar red shifts of 19 and 12 nm, respectively, with added imidazole.

At imidazole concentrations <0.02 M a series of isosbestic points at 375, 389, and 629 nm is observed. Inset A shows the isosbestic point at 389 nm. The presence of isosbestic points indicates that only two species, 4-coordinate NiDP-II and 5-coordinate ImNiDP-II, are present in this imidazole concentration range. A value of 10 ± 4 M^{-1} was calculated for K_1, as described in the Experimental Section.

At imidazole concentrations >0.60 M another series of isosbestic points is seen at 398, 414, 453, 512, and 634 nm. Inset B shows the isosbestic points at 398 and 414 nm. The presence

(26) Strauss, S. H.; Silver, M. E.; Long, K. M.; Thompson, R. G.; Hudgens, R. A.; Spartalian, K.; Ibers, J. A. *J. Am. Chem. Soc.* **1985**, *107*, 4207–4215.

(27) Disorder in the crystal prevents comparison of these bond lengths for the special-position molecule.

Table III. NiDP-II Fractional Monoclinic Coordinates and Isotropic Atomic Displacement Parameters (Å²)[a]

atom	x	y	z	B_{iso}
Ni	0.90413(2)	0.17399(2)	0.53809(2)	2.623(6)
N1	0.7725(1)	0.12704(9)	0.5792(1)	2.78(3)
N2	0.8196(1)	0.25925(9)	0.4878(1)	3.02(3)
N3	1.0376(1)	0.22239(9)	0.4962(1)	2.72(3)
N4	0.9870(1)	0.08831(9)	0.5880(1)	2.65(3)
C1a	0.7619(2)	0.0669(1)	0.6402(1)	2.95(4)
C2a	0.6681(2)	0.1453(1)	0.5559(1)	2.99(4)
C3a	0.7089(2)	0.2606(1)	0.4725(1)	3.32(4)
C4a	0.8611(2)	0.3278(1)	0.4583(1)	3.30(4)
C5a	1.0508(2)	0.2962(1)	0.4662(1)	3.11(4)
C6a	1.1379(2)	0.1855(1)	0.4924(1)	2.87(4)
C7a	1.0928(1)	0.0685(1)	0.5725(1)	2.67(3)
C8a	0.9519(2)	0.0325(1)	0.6460(1)	2.96(4)
C1b	0.6499(2)	0.0503(1)	0.6553(1)	3.13(4)
C2b	0.5920(2)	0.0971(1)	0.6005(1)	3.17(4)
C3b	0.6723(2)	0.3323(1)	0.4229(2)	3.93(4)
C4b	0.7746(2)	0.3788(1)	0.4230(2)	3.88(4)
C5b	1.1657(2)	0.3157(1)	0.4425(2)	3.42(4)
C6b	1.2198(2)	0.2377(1)	0.4568(1)	3.35(4)
C7b	1.1235(2)	−0.0005(1)	0.6198(1)	2.85(3)
C8b	1.0356(2)	−0.0221(1)	0.6668(1)	3.16(4)
C1m	0.6393(2)	0.2065(1)	0.5007(1)	3.46(4)
C2m	0.9678(2)	0.3476(1)	0.4524(2)	3.52(4)
C3m	1.1625(2)	0.1135(1)	0.5236(1)	2.92(4)
C4m	0.8467(2)	0.0252(1)	0.6735(1)	3.32(4)
C11	0.6090(2)	−0.0086(1)	0.7204(1)	3.51(4)
C12	0.6003(3)	−0.0897(2)	0.6829(2)	5.99(7)
C21	0.4712(2)	0.1041(2)	0.5909(2)	3.95(5)
C22	0.4238(2)	0.1652(2)	0.6519(2)	5.64(7)
C311	0.5801(2)	0.3774(2)	0.4673(2)	6.19(7)
C312	0.6037(3)	0.4020(2)	0.5616(3)	8.7(1)
C321	0.6395(2)	0.3104(2)	0.3280(2)	5.68(6)
C322	0.7237(3)	0.2666(2)	0.2766(2)	7.32(9)
O4	0.7866(1)	0.44539(9)	0.3973(1)	5.22(4)
C511	1.1771(2)	0.3433(2)	0.3467(2)	4.85(5)
C512	1.1267(3)	0.2902(2)	0.2776(2)	6.93(8)
C521	1.2158(2)	0.3767(1)	0.5048(2)	4.99(6)
C522	1.2256(3)	0.3528(2)	0.5994(2)	6.69(7)
O6	1.3152(1)	0.22299(9)	0.4447(1)	4.53(3)
C71	1.2315(2)	−0.0396(1)	0.6196(1)	3.39(4)
C72	1.2933(2)	−0.0325(2)	0.7072(2)	4.93(6)
C81	1.0247(2)	−0.0914(1)	0.7261(2)	4.33(5)
C82	1.0348(2)	−0.0710(2)	0.8246(2)	6.65(7)

[a] Estimated standard deviations in the least significant digits are given in parentheses. Thermal parameters for the anisotropically refined atoms are given in the form of the isotropic equivalent displacement parameter defined as $(4/3)[a^2B_{11} + b^2B_{22} + c^2B_{33} + ab(\cos\gamma)B_{12} + ac(\cos\beta)B_{13} + bc(\cos\alpha)B_{23}]$.

Table IV. NiTP-A Fractional Monoclinic Coordinates and Isotropic Atomic Displacement Parameters (Å²)[a]

atom	x	y	z	B_{iso}
Ni	0.13293(8)	0.14409(5)	0.06857(8)	2.78(2)
N1	−0.0208(4)	0.1820(2)	0.0156(4)	2.9(1)
N2	0.0722(4)	0.0941(2)	0.1660(4)	3.0(1)
N3	0.2820(4)	0.1064(2)	0.1167(4)	3.0(1)
N4	0.1938(4)	0.1914(2)	−0.0300(4)	2.9(1)
C1a	−0.0581(5)	0.2168(3)	−0.0728(5)	2.9(1)
C2a	−0.1092(5)	0.1792(3)	0.0683(5)	2.9(1)
C3a	−0.0272(5)	0.1041(3)	0.1984(5)	3.0(1)
C4a	0.1204(5)	0.0447(3)	0.2141(5)	3.6(2)
C5a	0.3062(5)	0.0542(3)	0.1704(6)	3.9(2)
C6a	0.3867(5)	0.1243(3)	0.1025(5)	3.4(2)
C7a	0.3089(5)	0.1992(3)	−0.0277(5)	3.2(1)
C8a	0.1253(5)	0.2220(3)	−0.1181(5)	3.7(2)
C1b	−0.1811(5)	0.2398(3)	−0.0872(5)	3.3(2)
C2b	−0.2112(5)	0.2129(3)	0.0096(5)	3.4(2)
C3b	−0.0441(5)	0.0607(3)	0.2751(5)	3.3(2)
C4b	0.0487(5)	0.0154(3)	0.2803(6)	4.8(2)
C5b	0.4276(6)	0.0394(3)	0.1896(6)	4.7(2)
C6b	0.4796(5)	0.0846(3)	0.1517(5)	3.9(2)
C7b	0.3231(6)	0.2393(3)	−0.1161(6)	4.9(2)
C8b	0.1982(6)	0.2487(3)	−0.1805(6)	5.0(2)
C1m	−0.1100(5)	0.1446(3)	0.1554(5)	2.9(1)
C2m	0.2277(6)	0.0237(3)	0.2110(6)	4.6(2)
C3m	0.4001(5)	0.1709(3)	0.0400(6)	3.8(2)
C4m	0.0090(5)	0.2317(3)	−0.1413(5)	4.0(2)
C111	−0.1777(6)	0.3059(3)	−0.0729(6)	5.4(2)
C121	−0.0954(9)	0.3277(4)	0.0324(8)	8.9(3)
C112	−0.2668(6)	0.2235(4)	−0.1974(6)	5.3(2)
C122	−0.2775(7)	0.1598(4)	−0.2181(7)	7.5(3)
O2	−0.3030(4)	0.2184(2)	0.0345(4)	4.6(1)
O3	−0.1205(4)	0.0588(2)	0.3228(4)	4.2(1)
C411	0.1177(7)	0.0033(4)	0.4034(7)	9.8(2)
C421	0.1687(9)	0.0560(7)	0.4654(8)	13.6(5)
C412	−0.0071(8)	−0.0395(4)	0.226(1)	13.0(3)
C422	−0.068(1)	−0.0375(6)	0.127(1)	8.9(5)
C423	−0.129(2)	−0.065(1)	0.214(2)	9.3(8)
C51	0.4843(6)	−0.0146(4)	0.2459(7)	6.0(2)
C52	0.523(1)	−0.0055(6)	0.3673(9)	12.2(4)
C61	0.6036(5)	0.0898(4)	0.1497(6)	4.8(2)
C62	0.6246(6)	0.0636(4)	0.0459(7)	7.0(2)
C711	0.3939(7)	0.2160(5)	−0.1876(7)	9.6(3)
C721	0.347(1)	0.1596(5)	−0.2413(8)	12.1(4)
C712	0.364(1)	0.3001(5)	−0.065(1)	14.6(4)
C722	0.418(2)	0.3422(8)	−0.114(2)	11.0(7)
C723	0.449(2)	0.3106(9)	−0.010(2)	10.6(7)
O8	0.1637(4)	0.2734(3)	−0.2692(4)	8.2(2)

[a] Estimated standard deviations in the least significant digits are given in parentheses. Thermal parameters for the anisotropically refined atoms are given in the form of the isotropic equivalent displacement parameter defined as $(4/3)[a^2B_{11} + b^2B_{22} + c^2B_{33} + ab(\cos\gamma)B_{12} + ac(\cos\beta)B_{13} + bc(\cos\alpha)B_{23}$.

of isosbestic points indicates that only two species, 5-coordinate ImNiDP-II and 6-coordinate Im_2NiDP-II, are present in this imidazole concentration range. A value of 7 ± 2 M^{-1} was calculated for K_2, as described in the Experimental Section.

Figure 6 shows that the electronic absorption spectrum of NiTP-A is substantially altered by the presence of imidazole. NiTP-A in CH_2Cl_2 (solid line) exhibits two strong bands in the Soret region at 356 and 430 nm and a third band at 471 nm. The spectrum with imidazole (dotted line) is substantially red-shifted with peaks at 442, 466, and 488 nm. NiTP-A in CH_2Cl_2 (solid line) shows several bands in the "Q band" region (624, 645, 661, and 680 nm) and a "red band" at 731 nm. The spectrum with imidazole (dotted line) exhibits blue-shifted bands in both the "Q band" (649 and 667 nm) and "red band" (704 nm) regions.

At imidazole concentrations $<3.3 \times 10^{-4}$ M a series of isosbestic points at 379, 671, 695, and 721 nm is observed for NiTP-A. Inset A (Figure 6) shows the isosbestic points at 695 and 721 nm. At imidazole concentrations $>4.9 \times 10^{-3}$ M another series of isosbestic points is seen at 671, 690, and 709 nm. Inset B shows the isosbestic point at 709 nm. Values of K_1 and K_2 for NiTP-A are 1700 ± 300 and 500 ± 150 M^{-1}, respectively, and were calculated analogously to those for NiDP-II.

Effect of Imidazole on $Ni^{3+/2+}$ Potentials in Ni β-Oxoporphyrins. Previous research from our laboratory established that one-electron electrochemical oxidation of NiDP-II and NiTP-A in acetonitrile solution occurs at the metal center, generating Ni^{III}DP-II and Ni^{III}TP-A.[6] We also showed that the $Ni^{3+/2+}$ potential in NiTP-A is sensitive to solvent, occurring 0.29 V more positive in methylene chloride than in acetonitrile solution.[6]

In the present work, we examined the effect of added imidazole on the $Ni^{3+/2+}$ potentials of NiDP-II and NiTP-A. The lowest potentials observed with added imidazole were 0.32 V vs SCE (approximately 2 M imidazole) and 0.27 V vs SCE (approximately 0.02 M imidazole) for NiDP-II and NiTP-A, respectively. These $Ni^{3+/2+}$ potentials are 0.26 V (NiDP-II) and 0.07 V (NiTP-A) less positive than those obtained in acetonitrile solution.

Discussion

Ni β-Oxoporphyrin Ring Ruffling Increases with Number of β-Oxo Groups. A convenient measure of the extent of ring ruffling, and hence the flexibility of a porphyrinic ring, is the methine carbon displacement from the four-nitrogen plane, d_m. These

Table V. Comparison of Selected Bond Distances (Å) and Bond Angles (deg) in 1–3[a,b]

	1			
	general	special	2	3
Ni–N_{sat}	1.973(3)	1.955(4)	1.957(9)	1.961(9)
Ni–N_{uns}	1.951(6)	1.939(3)	1.937(5)	1.919(4)
Ca–Cb (O)	1.466(5)	1.496(5)[c]	1.470(6)	1.457(4)
Ca–Cb (Et_2)	1.516(5)	1.496(5)[c]	1.511(2)	1.509(7)
Ca–Cb_{uns}	1.446(4)	1.431(9)	1.433(2)	1.440(2)
Cb–Cb_{sat}	1.520(5)	1.51(1)	1.504(8)	1.504(6)
Cb–Cb_{uns}	1.343(5)	1.355(22)	1.358(5)	1.371(8)
N–Ca	1.380(5)	1.369(9)	1.378(5)	1.371(5)
Ca–Cm	1.358(6)	1.366(21)	1.369(5)	1.366(4)
Cb–O	1.205(4)	1.255(9)	1.222(2)	1.221(1)
N–Ni–N_{adj}	90.1(2)	90.00(3)	90.00(19)	90.0(3)
Ni–N–Ca (Et_2)	127.2(2)	126.2(2)[b]	127.24(36)	127.3(2)
Ni–N–Ca (O)	125.3(2)	126.2(2)[b]	125.10(6)	124.9(3)
Ni–N–Ca_{uns}	128.0(1)	128.1(4)	127.90(17)	127.5(2)
Ca–N–Ca_{sat}	107.6(3)	107.6(4)	107.7(3)	107.8(12)
Ca–N–Ca_{uns}	104.1(3)	103.8(4)	104.20(22)	104.9(4)
Cm–Ca–Cb (Et_2)	121.3(3)	121.4(4)[b]	122.2(4)	122.3(4)
Cm–Ca–Cb (O)	120.6(3)	121.4(4)[b]	122.0(5)	122.3(1)
Cm–Ca–Cb_{uns}	124.5(4)	124.4(1)	124.5(3)	124.1(3)
N–Ca–Cm (Et_2)	125.6(4)	125.7(3)[b]	124.5(4)	124.4(3)
N–Ca–Cm (O)	127.4(3)	125.7(3)[b]	126.9(5)	126.2(4)
N–Ca–Cm_{uns}	124.3(3)	123.6(10)	124.0(2)	124.5(1)
Ca–Cm–Ca	125.0(5)	125.2(11)	124.0(2)	123.8(3)
Ca–Cb–Cb (Et_2)	101.6(3)	103.2(3)[b]	100.8(2)	100.8(4)
Ca–Cb–Cb (O)	105.7(3)	103.2(3)[b]	106.9(1)	106.7(2)
Ca–Cb–Cb_{uns}	106.8(6)	106.3(5)	106.6(1)	106.3(2)
N–Ca–Cb (Et_2)	113.1(3)	112.8(4)[b]	113.2(7)	113.1(3)
N–Ca–Cb (O)	112.0(3)	112.8(4)[b]	111.0(1)	111.1(4)
N–Ca–Cb_{uns}	111.2(3)	111.8(9)	111.3(2)	111.2(2)
Ca–Cb–O	127.5(3)	121.8(6)	126.4(9)	127.0(4)
Cb–Cb–O	126.8(4)	134.9(5)	126.7(8)	126.3(3)
Ca–Cb–C_{Et}	113.4(9)	115.9(25)	112.3(9)	112.4(9)
Cb–Cb–C_{Et}	110.2(9)	107.3(20)	110.7(4)	109.6(12)

[a] The esd of the mean was calculated as $[\sum_m(x_m - \bar{x})^2/n(n-1)]^{1/2}$. [b] Sat and uns refer to pyrrolinone and pyrrole rings, respectively. [c] These pairs of values are not distinguishable because of disorder in the crystal structure.

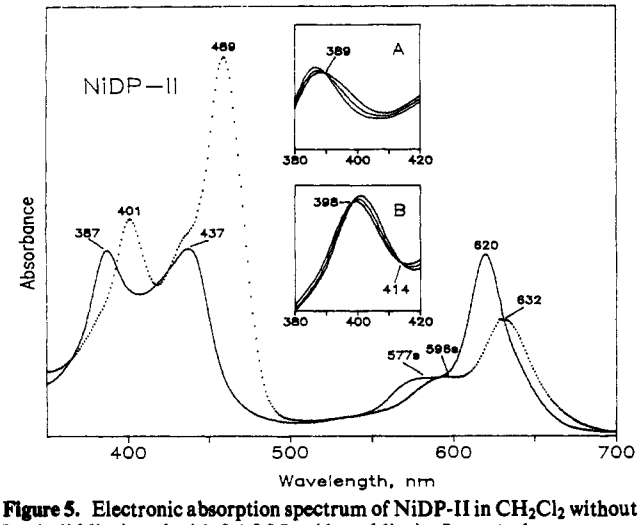

Figure 5. Electronic absorption spectrum of NiDP-II in CH_2Cl_2 without Im (solid line) and with 2.1 M Im (dotted line). Inset A shows spectra with low concentrations of imidazole (<0.02 M) from which K_1 was calculated. An isosbestic point is seen at 389 nm. Inset B shows spectra with high concentrations of Im (>0.60 M) from which K_2 was calculated. Isosbestic points are seen at 398 and 414 nm.

values increase with the number of β-oxo groups in the crystal structures of the Ni β-oxooctaethylporphyrin series: <0.10 Å (NiMP, general), 0.35 Å (NiMP, special), 0.45 Å (NiDP-II), 0.52 Å (NiTP-A). These values nicely correlate with the expected levels of aromaticity which result from the presence of one, two, or three β-oxo substituents. All three Ni β-oxoporphyrins exhibit less pronounced ruffling than NiTMC (0.58 Å)[17] and NiTMiBC

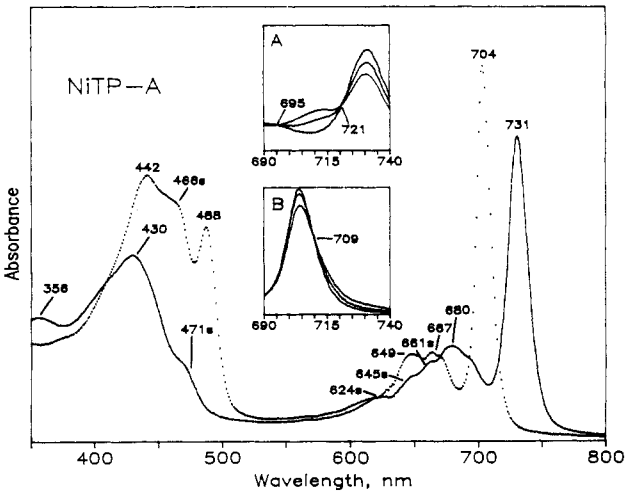

Figure 6. Electronic absorption spectrum of NiTP-A in CH_2Cl_2 without Im (solid line) and with 3.6×10^{-2} M Im (dotted line). Inset A shows spectra with low concentrations of imidazole (<3.3×10^{-4} M) from which K_1 was calculated. Isosbestic points are seen at 695 and 721 nm. Inset B shows spectra with high concentrations of Im (>4.9×10^{-3} M) from which K_2 was calculated. An isosbestic point is seen at 709 nm.

(approximately 0.66 Å),[18] indicating the flexibility of the β-oxoporphyrin rings is intermediate between those of chlorins and the typically planar[28] porphyrins. With the exception of the NiMP general-position molecule, the Ni β-oxoporphyrins examined have S_4 saddle-shaped ruffling, analogous to that observed[12a,14,17,18,26] in the structures of most Ni-containing reduced porphyrinic compounds. Ruffling decreases the typically too large core size of a reduced porphyrinic ring, which facilitates binding the small Ni ion.

The Montforts group has reported[11] the structure of the hematoporphyrin derivative of Ni dioxoporphyrin-II. Analogous saddle-shaped ruffling is seen, and a d_m value of 0.32 Å was calculated. It is not clear why the octaethylporphyrin derivative exhibits more extensive ruffling than observed in di-β-oxohematoporphyrin-II. The difference in structural parameters between di-β-oxohematoporphyrin-II and di-β-oxooctaethylporphyrin-II emphasizes the value of obtaining structures of the three β-oxo members within one series.

Two structures of di-β-oxooctaethylporphyrins with metals other than Ni have been reported.[7] CuDP-II[7b] exhibits significantly less ruffling than NiDP-II, with the largest methine carbon displacement being less than 0.15 Å. ClFeDP-II[7a] has been reported to have a domed structure with none of the methine carbons positioned above the four-nitrogen plane. Both of these structures are consistent with di-β-oxoporphyrin-II (DP-II) binding metals with larger radii than Ni(II), which do not require substantial ruffling as a mechanism for ring core contraction.

Strength of Ni β-Oxoporphyrin Imidazole Binding Increases with Number of β-Oxo Groups and Extent of Ring Ruffling. NiMP does not bind imidazole to a significant extent, as indicated by its essentially unchanged electronic absorption spectrum in the presence of high imidazole concentrations. NiDP-II exhibits imidazole binding with K_1 and K_2 values of 10 ± 4 and 7 ± 2 M^{-1}, respectively. NiTP-A binds imidazole ligands with K_1 and K_2 values of 1700 ± 300 and 500 ± 150 M^{-1}, respectively, approximately 10^2 times larger than those for NiDP-II. This is the same trend as observed by the Eschenmoser group[14] for the reduced porphyrinic series. They reported that the strength of axial ligation of methanol and acetonitrile increases in the following order, which parallels increasing d_m values: porphyrins

(28) (a) Brennan, T. D.; Scheidt, W. R.; Shelnutt, J. A. *J. Am. Chem. Soc.* **1988**, *110*, 3919–3924. (b) Scheidt, W. R.; Lee, Y. J. *Struct. Bonding* **1987**, *64*, 1–70. (c) Cullen, D. L.; Meyer, E. F. *J. Am. Chem. Soc.* **1974**, *96*, 2095–2102. (d) Hoard, J. L. *Ann. N.Y. Acad. Sci.* **1973**, *206*, 18–31.

< chlorins < isobacteriochlorins < bacteriochlorins < corphins < pyrrocorphins.[14]

Two conformational changes likely occur when Ni(II) β-oxoporphyrins bind axial ligands: (i) the porphyrinic core size increases, because electrons enter the antibonding $d_{x^2-y^2}$ orbital which expands the Ni(II) ion radius, and (ii) the porphyrinic ring flattens, since the core size enlarges. The structural mechanism for the parallel increases in ring ruffling and strength of imidazole binding in the Ni β-oxoporphyrins is the incremental increase in β-oxoporphyrin ring flexibility which results from saturation of each pyrrole ring.

NiTP-A Exhibits a Higher Affinity for Imidazole Than F430 and Positively Charged Porphyrins. Ni porphyrins do not bind imidazole unless positively charged groups are present on the porphyrin ring, which act to decrease the basicity of the porphyrin. An example is nickel *meso*-tetrakis(*N*-methylpyridiniumyl)porphyrin (NiTMPyP), which has a K_1 value of 8 M^{-1},[21] approximately the same as that for NiDP-II and 200 times smaller than that for NiTP-A.

Although the following discussion refers to data obtained with F430M,[20] it is assumed that the conclusions from F430M experiments represent the true nature of protein-bound F430. F430M binds imidazole with K_1 and K_2 values of 500 and 100 M^{-1}, respectively.[19] F430's high affinity for axial ligands has been attributed to the substantial flexibility of its tetrahydrocorphin ring, the presence of a positive charge on the tetrahydrocorphin ring, and two exocyclic electronegative C=O groups.[13,14]

Our results indicate that NiTP-A exhibits a higher affinity for imidazole than F430. This is surprising given that the F430M ring is more ruffled than that of NiTP-A (d_m = 0.78 Å[22] vs 0.52 Å) and F430 carries a positive charge while NiTP-A is uncharged. Ni(II)TP-A is oxidized at its metal center at 0.34 V vs SCE in acetonitrile solution, whereas the Ni(II) center of F430M is oxidized at 1.23 V vs SCE[16] in the same solvent. Observation of *both* a lower NiTP-A $Ni^{3+/2+}$ potential and a higher NiTP-A axial ligand affinity allows us to rule out ring basicity as the cause and to postulate that, conformationally, 4-coordinate NiTP-A is less stable than 4-coordinate F430. It follows that the former binds imidazole more strongly and requires a lower potential to generate Ni(III) due to the release of more conformational strain energy as the Ni becomes 6-coordinate and the porphyrinic ring flattens. It is conceivable that NiTP-A might experience greater conformational strain at 0.52-Å methine carbon displacement than F430M experiences at 0.78 Å, since the tri-β-oxoporphyrin ring is less saturated (and hence less flexible) than the F430 tetrahydrocorphin ring. It is important to keep in mind that the cause of ruffling is the same in both molecules: attainment of suitable Ni–N distances. Conformational instability has been used to rationalize the fact that F430 has higher axial ligand affinity than its 12,13-diepimer.[12f] A less stable conformation of corphin ring substituents exists in the former, which destabilizes the 4-coordinate relative to the 5- and 6-coordinate species.

$Ni^{3+/2+}$ Potentials in NiDP-II and NiTP-A Shift in the Negative Direction with Imidazole. $Ni^{3+/2+}$ potentials in NiDP-II and NiTP-A in methylene chloride are sensitive to imidazole concentration, shifting in the negative direction as imidazole is added. The direction of the shift indicates that axial ligation of imidazole preferentially stabilizes Ni(III) over Ni(II),[29] which is reasonable in view of the greater electrophilicity of the former. The lowest potentials observed for the $Ni^{3+/2+}$ couples of NiDP-II and NiTP-A with imidazole present are 0.32 V (approximately 2 M imidazole) and 0.27 V (approximately 0.02 M imidazole) vs SCE, respectively.

$Ni^{3+/2+}$ potentials are very similar for NiTP-A in acetonitrile (0.34 V) and imidazole/methylene chloride (0.27 V). In contrast, $Ni^{3+/2+}$ potentials of NiDP-II differ by 0.26 V under these conditions, 0.58 V (acetonitrile) vs 0.32 V (imidazole/methylene chloride). It is not possible to compare NiDP-II and NiTP-A potentials in pure methylene chloride, since NiDP-II is oxidized at the porphyrinic ring, rather than the Ni center, in this solvent.[6] The substantially lower $Ni^{3+/2+}$ potential for NiDP-II in imidazole/methylene chloride solution versus that in acetonitrile suggests that Ni^{III}DP-II binds imidazole significantly more strongly than it binds acetonitrile. In contrast, the similar $Ni^{3+/2+}$ potentials for NiTP-A in the two systems indicate that Ni^{III}TP-A is stabilized relative to Ni^{II}TP-A only slightly more by imidazole than by acetonitrile.

Ligand-binding studies were attempted by Jaun[16] with F430M, but the high oxidation potential (1.23 V vs SCE) precluded reversible cyclic voltammograms due to appreciable imidazole oxidation. Jaun has suggested that an axially coordinated form of Ni(III) F430 might be a possible biological intermediate, since the $Ni^{3+/2+}$ potential could be lowered substantially by axial ligation. Our results show that Ni(II)TP-A is oxidized to Ni(III) at the low potential of 0.27 V in the presence of imidazole, 0.36 V lower than the value for $Ni^{3+/2+}$ oxidation in methylene chloride solution, where the only possible axial ligand is the electrolytic anion, perchlorate. This result illustrates the powerful modulation of $Ni^{3+/2+}$ potentials which can be accomplished by a biologically relevant porphyrinic ligand.

β-Oxo Groups Have Ability To Either Decrease or Increase Metal Oxidation Potentials. Previous work from our laboratory demonstrated that site of oxidation (metal versus porphyrinic ring) and $Ni^{3+/2+}$ potentials are sensitive to the number of β-oxo ring groups.[6] The $Ni^{3+/2+}$ potential in acetonitrile is 0.24 V less positive for NiTP-A than for NiDP-II. In addition, the β-oxoporphyrins exhibit the *lowest* potentials for Ni oxidation within the porphyrinic series (porphyrins, chlorins, isobacteriochlorins, etc.).[6]

In contrast to our studies reporting lower potentials for metal oxidation in Ni β-oxoporphyrins, the work of Fajer[7b] has nicely shown that Fe β-oxoporphyrins exhibit more positive potentials for $Fe^{3+/2+}$ oxidation as the number of β-oxo groups increases. Furthermore, the $Fe^{3+/2+}$ potentials for Fe β-oxoporphyrins are among the *highest* within the porphyrinic series.

Fajer, Barkigia, and co-workers[7a] attributed the increasing $Fe^{3+/2+}$ potentials to the electron-withdrawing effect of the β-oxo group. We have rationalized the decreasing $Ni^{3+/2+}$ potentials on the basis of added flexibility arising from each β-oxo group.[6] This flexibility facilitates the core size alterations which accompany both Ni oxidation and any concomitant axial ligation changes.

β-Oxoporphyrin rings apparently modulate bound metal redox potentials by both mechanisms. Which mechanism predominates depends on the extent of the porphyrinic ring conformational change involved in the redox process. If a large core size change dictates a substantially altered porphyrinic ring structure, the more flexible ring will undergo the redox change with a lower potential. However, if a small conformational change is involved, porphyrinic basicity will dominate the redox potential trend, with the more electron-poor porphyrinic ring being oxidized at a more positive potential. The former situation exists for Ni(II) oxidation, whereas the latter case describes the $Fe^{3+/2+}$ couple.

Fajer, Barkigia, and co-workers have suggested two plausible biological roles for the C=O groups of heme-d_1: (i) modulation of the metal redox properties via the electron-withdrawing effect of the C=O groups and (ii) anchoring the prosthetic group to nearby protein residues.[7a] Our results with Ni β-oxoporphyrins illustrate the structural flexibility of the di-β-oxoporphyrin ring and emphasize that porphyrinic structural flexibility can affect redox potentials when conformational changes accompany a redox reaction. In view of the substantial flexibility of DP-II, an additional possible biological role for the heme-d_1 di-β-oxopor-

(29) Bottomley, L. A.; Kadish, K. M. *Inorg. Chem.* **1981**, *20*, 1348–1357.

phyrin ring is to facilitate *local* distortion of the heme-d_1 ring in the enzyme. Such distortion might be required for hydrogen bonding or result from steric constraints of the enzyme tertiary structure, and it could also be a mechanism for heme-d_1 redox potential and/or axial ligation modulation.

Acknowledgment. We express our appreciation to Dr. Mary T. Hertrich (Ohio Dominican College) for the generous use of the Bausch and Lomb spectrophotometer and for helpful discussions concerning the spectrophotometric titration experiments. We also express our gratitude to Dr. Andreas Pfaltz (Institute for Organic Chemistry, University of Basel) for sending us information on the F430M imidazole spectrophotometric titrations. We thank the University of Notre Dame for a Reilly Fellowship awarded to P.A.C. Acknowledgment is made to the donors of the Petroleum Research Fund, administered by the American Chemical Society, for support of this research.

Supplementary Material Available: Tables of hydrogen atom coordinates, anisotropic atomic displacement parameters, bond distances, bond angles, and least-squares planes for each structure (20 pages). Ordering information is given on any current masthead page.